

# Field-induced charge-density-wave transitions in the organic metal $\alpha$ -(BEDT-TTF)<sub>2</sub>KHg(SCN)<sub>4</sub> under hydrostatic pressure

D. Andres<sup>1</sup>, M. V. Kartsovnik<sup>1</sup>, W. Biberacher<sup>1</sup>, K. Neumaier<sup>1</sup>, I. Sheikin<sup>2</sup>, and H. Müller<sup>3</sup>

<sup>1</sup>*Walther-Meissner-Institut, Bayerische Akademie  
der Wissenschaften, D-85748 Garching, Germany*

<sup>2</sup>*High Magnetic Field Laboratory, CNRS, F-38042 Grenoble France and*

<sup>3</sup>*European Synchrotron Radiation Facility, F-38043 Grenoble, France*

## Abstract

Successive magnetic-field-induced charge-density-wave transitions in the molecular conductor  $\alpha$ -(BEDT-TTF)<sub>2</sub>KHg(SCN)<sub>4</sub> are studied in the hydrostatic pressure regime, in which the zero field charge-density wave (CDW) state is completely suppressed. The orbital effect of the magnetic field is demonstrated to restore the density wave, while the orbital quantization induces different CDW states in different field intervals. In particular, we have found that at certain field orientations the hysteretic first order transitions between field-induced CDW subphases become visible at much higher temperatures. This observation is very well in line with the existing theories of field-induced CDW transitions.

## I. INTRODUCTION

Phase transitions in low-dimensional molecular conductors induced by rather high magnetic fields have become an intensively studied topic during the last two decades<sup>1</sup>. Among the most prominent examples are the field-induced transition to a spin-density-wave state<sup>1,2</sup> or, recently discovered, the field-induced superconductivity<sup>3,4</sup>. The former effect in strongly anisotropic quasi-one dimensional (Q1D) electron systems has its origin in an effective reduction of the dimensionality due to the orbital motion of charge carriers in magnetic field on open sheets of the Fermi surface<sup>5</sup>, therefore being called orbital effect.

In the layered organic metal  $\alpha$ -(BEDT-TTF)<sub>2</sub>KHg(SCN)<sub>4</sub> there exists a charge-density-wave (CDW) state below 8 K at ambient pressure<sup>6,7,8,9</sup>. A Q1D electron band becomes gapped at the Fermi level, due to the so-called nesting of the Fermi surface, while the other, quasi-two-dimensional (Q2D) band still determines a metallic character of the system.

It has been found, that hydrostatic pressure deteriorates the nesting conditions and even leads to a complete suppression of the density-wave at  $P_0 \approx 2.5$  kbar<sup>10,11</sup>. The suppression is easily explained by an increase in the dimensionality of the Q1D band with hydrostatic pressure or correspondingly an increase of the ratio between the effective nearest and next-nearest interchain hopping integrals  $t_c/t'_c$  within the conducting **a-c** plane. The complete suppression of the CDW state at  $P_0$  has also been demonstrated to be directly reflected in a distinct impact on another, superconducting state also existing in this compound<sup>11</sup>.

Remarkably, it was shown that the orbital effect of magnetic field exists in this CDW system<sup>10</sup>. By applying a magnetic field, oriented along the least conducting direction, it is possible that the imperfectly nested CDW state, at  $P=1.5-2.5$  kbar, even becomes stabilized before the suppression by the additional, Pauli paramagnetic effect sets in.

Further, it was found that effects of orbital quantization take place in the present compound<sup>12</sup>, where the nesting vector appears to shift or jump between quantized values on changing the magnetic field. Qualitatively, this effect emerges, if the nesting conditions of the Fermi surface become so bad that free carriers would start reappearing on the 1D sheets of the Fermi surface<sup>1</sup>. In the present case it was found that within the high field CDW<sub>x</sub> state, existing above the paramagnetic limit<sup>6,7,12,13</sup>, the Pauli effect takes this unnesting role<sup>12</sup>. This in turn suggests that strong worsening of the nesting conditions by hydrostatic pressure also realizes orbital quantization effects<sup>14,15</sup>.

The situation is fairly similar to the well known SDW systems of the Bechgaard salts<sup>1</sup>. In those compounds, all carriers on the open sheets of the Fermi surface can be considered to be completely gapped up to the critical pressure, while above they would become free, that eventually completely suppresses the density wave. In a magnetic field, best oriented along the least conducting direction, it is then possible to again stabilize the density wave<sup>16,17,18</sup>. However, there will now be quantized values of the nesting vector most preferable which lead to different SDW subphases<sup>1,5,16,19,20,21</sup> in different field ranges. On going from one subphase to another one the nesting vector shifts to another quantized level. At low enough temperatures this shift even turns to an abrupt jump that causes the phase transition to change from the second to the first order. Similar effects under hydrostatic pressure, namely field-induced CDW (FICDW) transitions, have already been proposed to occur in this organic CDW compound<sup>15</sup>. However, besides some hints noted in our previous reports<sup>10,22,23,24</sup>, these phenomena are still lacking experimental proof.

In this work we give direct experimental evidence that first order FICDW transitions indeed exist under pressure. This is especially demonstrated by distinct hysteretic structures in the magnetoresistance, at sweeping the magnetic field up and down. In particular, it is shown that, by tilting the magnetic field towards the conducting plane, it is even possible to shift the onset temperature of the FICDW first order transitions to much higher values. This observation is shown to be in line with recent theoretical models of the FICDW phenomenon.

## II. EXPERIMENT

We have performed standard four point measurements of the interlayer resistance. The typical sample resistances at room temperature were  $\sim 10^3 - 10^4 \Omega$  with contact resistances of  $\sim 30\Omega$ . Overheating of the samples was always checked to be negligible by choosing appropriate measuring currents, that e.g. turned out to be as low as 100 nA at 100 mK.

To apply pressure, a big ( $\varnothing=20\text{mm}$ ) and a small ( $\varnothing=10\text{mm}$ ) BeCu clamp cells were used. The pressure at low temperatures was determined from the resistance of a calibrated manganin coil to an accuracy better than  $\pm 100$  bar. The temperature was monitored by the resistance of a RuO sensor below 0.3 K. The big cell was mounted on the cold finger of a home made dilution refrigerator, the sample being oriented so that its conducting ac-plane was perpendicular to the magnetic field generated by a superconducting magnet. In order to

keep the lowest operating temperature of 100 mK, the rate of the field sweeps were chosen as small as 2 mT/sec. Further, at the lowest temperatures weak demagnetization effects of the pressure cell became significant and had to be taken into account at controlling the temperature. All in all, the lowest temperature could be kept constant during a field sweep up to 15 T to an accuracy of  $\leq 10\%$ .

Effects of field orientation were studied in the 28 T resistive magnet at the HMFL in Grenoble using the small pressure cell. The cell was mounted on a  $^3\text{He}$  two-axes rotation insert. The absolute values of both angles determining the sample orientation could be determined to an accuracy better than  $0.5^\circ$ , and changed with the resolution better than  $0.05^\circ$ . Field sweeps at fixed field orientations were made at temperatures down to 0.4 K. The angle-dependent magnetoresistance at fixed field intensities was measured by sweeping the polar angle  $\theta$  at different azimuthal angles  $\varphi$ . At reasonable sweep rates of  $\sim 0.1^\circ/\text{sec}$  the lowest achievable temperature was 0.7 K.

### III. RESULTS AND DISCUSSION

#### A. The re-entrant CDW state under pressure

The critical pressure  $P_0$ , at which the zero-field density-wave transition becomes fully suppressed has been determined as  $2.5 \pm 0.1$  kbar<sup>10,11</sup>. Above  $P_0$  we expect the CDW state only to become stabilized via the orbital effect of magnetic field. Fig. 1 shows magnetic field sweeps up to 15 T, with the field directed perpendicular to the conducting plane, at 100 mK for different pressures covering the whole pressure range investigated within this work. The data presented in Fig. 1 are obtained on one and the same sample and have been qualitatively reproduced on another one measured at the same time. Since the pressures were applied successively, i.e., without opening the clamp cell, the magnetic field orientation is exactly the same for each pressure.

One of the basic characteristics of the ambient-pressure CDW state of the present compound is the strong magnetoresistance,  $R(10\text{ T})/R(0\text{ T}) \sim 10^2$  at low  $T$ , most likely caused by a reconstruction of the closed orbits of the Q2D carriers in the presence of the CDW potential<sup>25,26</sup>. At  $\approx 11$  T the magnetoresistance has a maximum followed by a negative slope associated with a reentrance to the closed orbit topology due to magnetic breakdown<sup>26</sup>

between the strongly warped open sheets of the Fermi surface. The latter also allows the fast Shubnikov-de Haas (SdH) oscillations at frequency  $F_\alpha = 670$  T corresponding to the undisturbed Q2D band to appear. Moreover, it is known, that there is an anomalously strong second harmonic signal at  $2F_\alpha$  as well as additional SdH frequencies at  $F_\lambda = 170$  T and  $F_\nu = F_\alpha + F_\lambda$ , which only appear in the CDW state. The origin of these unexpected frequencies is still under debate<sup>25,27,28,29</sup>.

Under pressure, the magnitude of the magnetoresistance in Fig. 1 becomes smaller that is related to the gradual suppression of the CDW energy gap. Besides this, the curves show other pressure-induced changes, in particular on crossing the critical pressure  $P_0$ . Most significantly, at pressures  $P \gtrsim P_0$  slow oscillations emerge in the magnetoresistance background. With increasing pressure these oscillations gradually move up in field that is visualized by the dashed lines in Fig. 1. Their amplitude is maximum at 3-3.5 kbar and reduces at further increasing pressure. Obviously, these slow oscillations occur exactly in the pressure range, in which FICDW transitions are expected, i.e. at  $P > P_0$ .

Another distinct change on crossing the critical pressure is the field at which the fast oscillations start to become visible. While at  $P < P_0$  these oscillations appear at rather high fields, shortly before the magnetoresistance background reaches the maximum, i.e. 5-7 T, they already start below 2 T at  $P > P_0$ . This is directly seen in Fig. 2, where the field sweeps around 2 T are shown in an enlarged field scale at pressures above and below 2.5 kbar.

To better understand these changes at  $P > P_0$ , it turns out to be useful to take a closer view on how the slow oscillations develop on lowering the temperature. In Fig. 3 field sweeps taken at 3 kbar are shown for different temperatures. At 4.2 K the resistance increases rather moderately with field and no sign of any anomaly is seen. We therefore consider the normal metallic state at this temperature to be present over the whole field range. At 2.5 K, a stronger enhancement of the magnetoresistance starting from  $\approx 6$  T indicates the reentrance into the CDW state. The orbital effect establishes the density-wave state. With lowering the temperature the enhancement of the magnetoresistance shifts to lower fields. Remarkably, the slow oscillations only appear in the field region where the magnetoresistance is elevated. This strongly suggests that the slow oscillations only exist within the re-entrant CDW state.

Within the whole temperature range the slope of the magnetoresistance below 2 T remains

approximately the same. Moreover, in this field and pressure range the resistance turns out to be even nearly temperature independent below 1 K as can be seen from Fig. 4, where the field sweeps at 0.1 and 1 K are shown at  $P = 3.5$  kbar. This coincides very well with the previous observation that the normal metallic state exists at low fields at  $P > P_0 = 2.5$  kbar<sup>11</sup>. The cylindrical orbits on the Fermi surface of the Q2D carriers are then undisturbed, i.e. no breakdown gaps exist anymore. Hence, it becomes clear why the  $\alpha$ -oscillations start at such low fields, as shown in Fig. 2.

The presence of the CDW state at higher fields at  $P > P_0$  is directly reflected in its distinct properties: First, in the field range of 10-15 T the additional SdH frequencies  $F_\lambda$  and  $F_\nu$ , characteristic of the CDW state, are observed. An example of the Fast-Fourier-Transformation (FFT) spectrum of the magnetoresistance at 3.5 kbar is given in Fig. 5. Surprisingly, the frequency  $F_\lambda$  is found to be pressure independent, unlike  $F_\alpha$  which in our studies shows a pressure dependence of 17 T/kbar. Second, there is a broad hysteresis in the magnetoresistance between up- and downward sweeps of the magnetic field at  $B \geq 3$  T. In Fig. 3 up and down sweeps of the magnetic field are plotted for the lowest temperature, where the broad hysteresis is clearly seen. Such a hysteresis is definitely inconsistent with a normal metallic behavior. On the other hand, it is known to be present in the CDW state of this compound<sup>30</sup>. Third, on lowering the temperature a strong decrease of the magnetoresistance background is observed at  $B \gtrsim 8$  T, as can be seen in Fig. 4. This is combined with a phase inversion of the fast  $\alpha$  oscillations as marked in Figs. 3 and 4 for 3 and 3.5 kbar, respectively, by vertical dashed lines. Such a behavior has already been found to occur deep in the CDW state and was discussed in a number of publications<sup>22,31,32,33</sup>.

Altogether, the reentrance to the CDW state in magnetic field at pressures between 2.5 and 4 kbar is clearly seen in the magnetoresistance data. The measured phase transition fields and temperatures are qualitatively well described by the theoretical  $B$ - $T$  phase diagrams of a Q1D CDW system at different nesting conditions, which were proposed by Zanchi et al.<sup>14</sup>.

Now we turn to the origin of the slow oscillations which exist only in the re-entrant CDW state. At first glance one can suppose that these are SdH oscillations emerging due to small pockets on the Fermi surface, induced by imperfect nesting. This would give a SdH signal of a very low frequency in  $1/B$ . Indeed, a FFT transformation in the whole, inverted, field range within the re-entrant CDW state shows a peak at about 20 T. The spectra of the

oscillations given in Fig. 1 are shown in Fig. 6. Since these peaks are deduced from only very few oscillation periods it is hard to judge about their exact positions. Moreover, since the magnetoresistance background in the CDW state is not known and was evaluated by a low order polynomial fit, an artificial shift of the peak positions  $\leq 1$  T might arise in the FFT spectrum. We therefore cannot judge about the pressure dependence of the low frequency. Nevertheless, a periodicity of these oscillations in  $1/B$  is clearly reflected. However, as will be pointed out below, there are several observations which contradict the theory of the normal quantum SdH oscillations, and favor the existence of FICDW transitions.

### B. Field-Induced CDW Transitions at Perpendicular Field

Fig. 7 shows the magnetoresistance obtained from the up- ( $R_B^\uparrow$ , black curve) and downward ( $R_B^\downarrow$ , grey curve) sweeps of magnetic field at  $P = 3$  kbar,  $T = 0.1$  K. The raw magnetoresistance at increasing field is shown in the figure by the dotted grey line. The lower curve in Fig. 7 shows the difference  $\Delta R = R_B^\downarrow - R_B^\uparrow$  between the up and down sweeps, demonstrating a considerable hysteresis, that was already mentioned above in Sec. IIIA. The hysteresis exhibits a clear structure correlated with the slow oscillations of the magnetoresistance background: its maxima are located at approximately the field values corresponding to the maximum curvature in  $R_b(B)$ .

Another peculiarity of the slow oscillation is the temperature dependence of the phase. To illustrate the temperature dependence of the phase of the slow oscillation, dashed lines following the maximum curvature of the slow oscillations are placed into Fig. 3. This anomalous behavior is certainly not expected for normal SdH oscillations. On the other hand, the curves themselves, however, are qualitatively quite similar to those observed in the FISDW states of the Bechgaard salts<sup>34,35</sup>.

There are further similarities to the FISDW transitions, such as for example the pressure dependence of the transition fields shown in Fig. 8. The FICDW transition fields were defined from Fig. 1 as the fields of maximum curvature of the magnetoresistance background. Such a choice looks reasonable since these points also correspond to the maxima in the hysteresis structure at 3 kbar. The obtained transition fields at 100 mK move approximately linearly to higher values with enhancing the pressure. Note, however, that this shift with pressure is quite strong. For SdH oscillations, this would correspond to an expansion of the Fermi

surface orbit area by about 20%/kbar. The resulting increase of the SdH frequency must therefore be clearly resolved in the FFT spectrum. Since this is not the case here, this gives another argument against the usual SdH effect as the reason for the observed slow oscillations. On the other hand, a shift of the FISDW transitions to higher fields with increasing pressure, or increasing  $t'_c$ , has already been demonstrated experimentally<sup>36</sup> on the Bechgaard salts. Thus, the observed behavior is consistent with what one would expect for FICDW.

In the whole, we regard these observations as a sign of first order transitions between the FICDW subphases. Unlike the sharp, well defined hysteretic FISDW transitions<sup>35</sup>, the transitions in our compound as well as the peaks in the hysteresis are found to be smeared. The hysteretic first order transitions obviously appear only at such low temperatures,  $T \sim 0.1$  K. Hence, relative to the ambient pressure density-wave transition temperature, these first order FICDW transitions exist in a much lower temperature range in comparison to the known FISDW cases of the Bechgaard salts. Indeed, this is exactly what has been predicted by Lebed<sup>15</sup>. The reason for this comes from the fact that in the CDW the nesting vector couples carriers of the same spin band<sup>8,37,38</sup>. That effectively causes the paramagnetic suppression of the CDW at high fields<sup>14,39,40,41</sup> and also has to be taken into account in the FICDW regime. Actually, the quantization condition of the nesting vector must be extended by an additional Zeeman or Pauli term<sup>15</sup>:

$$Q_x = 2k_F \pm q_{x,\text{Pauli}} + q_{x,\text{orb}} = 2k_F \pm \frac{2\mu_B B}{\hbar v_F} + N \cdot G; \quad N = 0, \pm 1 \pm 2 \dots \quad (1)$$

$$G = \frac{2ea_y B_z}{\hbar}$$

$Q_x$  being the nesting vector component in the conducting chain direction,  $k_F$  the Fermi wave vector,  $\mu_B$  the Bohr magneton,  $v_F$  the Fermi velocity of the Q1D part of the electron system,  $a_y$  the lattice parameter perpendicular to the conducting chains within the layer and  $B_z$  the field component perpendicular to the conducting planes. The right hand side of Eq. (1) is equivalent to two sets of quantized levels, one for each spin subband. If the quantized values for both spin bands do not match each other, the effective CDW coupling constant decreases, and so does the transition temperature of the FICDW state, as well as the onset temperature of the first order transitions.

Finally, we note that a modulation of the SdH oscillation amplitude of the  $\alpha$  frequency in the FICDW states is observed at the lowest temperature (see Fig. 1). Its nature, however, is

unclear at present. No direct correlation between the modulation and the FICDW transitions has been found so far. Further measurements are needed to draw any reliable conclusions.

The discussion of Eq. (1) showed that the mismatch of the quantized levels for different spin bands is the reason for the suppression of the onset temperature of the first order transitions. As we will show next there is a possibility to enhance the density wave instability, by changing the magnetic field orientation.

### C. FICDW transitions at different orientations of magnetic field

An important consequence of tilting the field by an angle  $\theta$  from the perpendicular direction towards the conducting plane is the following: while the Zeeman spin splitting can be considered as an isotropic effect, the orbital quantization depends only on the field component perpendicular to the conducting planes,  $B_z = B \cos \theta$ . On tilting the field the quantized levels of each spin subband therefore move closer to each other but the distance between the  $N = 0$  levels of the subbands,  $\mu_B B / \hbar v_F$ , remains the same. At certain angles one, therefore, expects the quantized spin-up levels to coincide with the spin-down ones. For such "commensurate splitting" (CS) angles the re-entrant CDW is predicted to become stabilized at higher temperatures<sup>15,42</sup>.

In Fig. 11 the scaled field sweeps for different angles, covering a wide angular range, are shown. Obviously, the amplitude of the slow oscillations is strongly angle dependent. In this angle interval,  $0^\circ - 74^\circ$ , there are two regions, around  $57^\circ$  and  $71^\circ$ , where the amplitude of the slow oscillations has a maximum, whereas around  $43^\circ$  and  $65^\circ$ , it nearly vanishes. Besides this angular oscillation of the amplitude, the transition fields also provide some information: on crossing the angle where the amplitude nearly vanishes, the transition fields shift by half a period. The dashed lines in Fig. 11 mark the transition fields, where the oscillation has a maximum curvature. As can be seen, the transition fields change several times their positions on tilting the magnetic field. Thus, the slow oscillations are found to possess some kind of "spin zeros" at certain field directions, as known from the normal SdH effect. In the latter effect the phase of the oscillations inverts several times on tilting the magnetic field<sup>43,44</sup>.

To understand this behavior in the present case of field-induced CDW transitions, we first have to recall in a qualitative manner what happens in a SDW system. In the FICDW

pressure range there are preferable, quantized values of the  $x$  component of the nesting vector. The spin susceptibility or response function  $\chi(Q_x)$  of the system therefore is a more or less periodic function with maxima at such values of the nesting vector<sup>20</sup>. At not too low temperatures we assume this response, expanded into a harmonic series, to be strongly dominated by its first harmonic. If we now switch to the CDW system, one has to consider the Zeeman energy splitting of the different spin bands.

Assuming the response in the CDW system of each spin band also to be well described by its first harmonic, the situation resembles the Landau quantization. The superposition of both response functions gives a total oscillating response function, where the phase keeps the same at a constant out-of-plane field component,  $B \cos \theta$ , independent of the field orientation. However, the sign of the oscillation may change, that determines a phase inversion. The same mechanism leads to the spin zeros in the quantum SdH and de Haas-van Alphen effects. This means that since the orbital quantization only depends on the magnetic field component in the least conducting direction, there is the possibility that by tilting the magnetic field the oscillation of the response function inverts its phase. Since the quantized values are determined by the maxima of the total response function, these quantized values will shift by half a period. Hence, one can also expect the FICDW transitions to shift in magnetic field. Noteworthy, we do not expect the same effect to happen in SDW systems, since in the latter the nesting vector is not influenced by the Pauli effect.

In the picture described above, a change of the FICDW transition fields should happen at exactly those angles at which quantized values of the nesting vector, Eq. (1), for one of the spin subbands lie exactly in the middle between those of the other spin subband. These angles are easily derived to be determined by:

$$\cos(\theta) = \frac{1}{M + 0.5} \left[ \frac{2\mu_B}{v_F e a_c} \right]; \quad M = \pm 1, \pm 2, \dots \quad (2)$$

Another interesting observation is shown in Figure 9, where magnetic field sweeps, with the field scaled in  $\cos \theta$ , are shown at different angles in the narrow interval  $\theta = 50^\circ - 60^\circ$  at 2.8 kbar. The black curves are taken on sweeping the field up, grey curves on sweeping down. Obviously, the slow oscillations do scale in  $\cos \theta$ . This is expected, since the quantization is determined by the field component  $B_z = B \cos(\theta)$ . As in the case of the perpendicular oriented field at 3 kbar, see Fig. 7, a modulated hysteresis between both sweep directions with rather sharp peaks is observed. This can be directly seen in Fig. 10 where the magnitude of

the hysteresis is plotted against the field for different tilt angles. Within this angular range this hysteresis becomes strongest at the field-induced transition marked by the dashed line in Fig. 9. Further, it is seen from Fig. 10 that at  $57.7^\circ$  the magnitude of this hysteresis has a maximum. Note that the temperature here,  $T = 0.45$  K, is much higher than for the data in Fig. 7; at perpendicular field direction no structure in the hysteresis, corresponding to the different FICDW transitions, has been resolved.

The fact that this hysteretic structure was only observed in this narrow angular range, makes us believe that this is an effect of the first CS angle. As mentioned at the beginning of this section, at the CS angles the total CDW susceptibility becomes stronger and the coupling constant as well as the transition temperature of the density wave should increase<sup>15</sup>.

Thus, altogether, if we know the angles where the phase of the slow oscillations changes, there is then the possibility to directly evaluate the CS field orientations, i.e. the directions, where the first order transitions should appear at higher temperatures. These must be given by<sup>15,42</sup>:

$$\cos(\theta) = \frac{1}{M} \left[ \frac{2\mu_B}{v_F e a_y} \right]. \quad (3)$$

In our experiment many field sweeps were performed at different angles. Since the angular step was chosen rather small, the first three ranges, in which the sign reversal of the slow oscillation occurs, are found to be restricted to the narrow intervals:

$$\theta_{S1} = 40^\circ - 45^\circ, \theta_{S2} = 63.7^\circ - 65.7^\circ \text{ and } \theta_{S3} = 73^\circ - 73.9^\circ.$$

These angular intervals are in good agreement with the assumed  $1/\cos(\theta)$  scaling, Eq. (2), as can be seen in Fig. 12 where the commensurability index is plotted against  $1/\cos(\theta)$ . The corresponding Fermi velocity amounts to  $\approx 1.2 \cdot 10^5$  m/sec, that is about twice the value determined at ambient pressure by Kovalev et al.<sup>45</sup>:  $0.65 \cdot 10^7$  cm/sec.

From Eq. (3) and Fig. 12 the first CS angle may thus be evaluated to:  $\theta_{c1} = 55.60^\circ - 58.97^\circ$ ; i.e. exactly the angular range where we find a pronounced increase in the hysteresis, see Fig. 10. This remarkable agreement between our experimental results and this simple model above gives another strong argument for the existence of FICDW subphases at  $P \geq P_0$ .

Noteworthy, from Fig. 12 it follows that at perpendicular field direction we are by far not at a CS angle, so that here the coupling constant must be rather low. This explains why at this field orientation the hysteretic first order transitions appear at much lower temperatures than at the CS angles.

#### D. Angle dependent magnetoresistance

Now that the general behavior under pressure is qualitatively understood, we discuss the effects which can be seen in the angle-dependent magnetoresistance oscillations (AMRO) at  $P > P_c$ .

The field orientation is always turned in a plane normal to the layers and the angle  $\theta$  is determined as before. The measurement of AMRO is a powerful tool to determine the Fermi surface in such low-dimensional electron systems<sup>46</sup>. For the present compound the AMROs in the CDW state well describe strongly warped open orbits, which are effectively created by the Q2D electrons being exposed to the CDW potential<sup>25</sup>. They show pronounced dips, periodic in  $\tan \theta$ , in the otherwise rather high magnetoresistance. We will refer to this kind of AMRO as the "Q1D type". By contrast, in the NM state the AMRO are of the "Q2D type", i.e. mostly determined by the cylindrical part of the Fermi surface, showing pronounced peaks in the magnetoresistance, also periodic in  $\tan(\theta)$ . Therefore, a field-induced transition from the NM to the CDW state should also be resolved in AMRO measurements.

A set of AMROs measured at 2.8 kbar and 0.7 K is shown in Fig. 13. The superposed fast oscillations developing at  $B \geq 6.5$  T are SdH oscillations. These curves were measured in the same cooling run as the data shown in Figs. 9 and 11, i.e., the pressure was exactly the same. At 1 T, the AMRO, although very weak, shows a normal metallic behavior, as expected from our discussion above. On enhancing the field, see 4.3, 6.5 and 9 T curves in Fig. 13, the magnetoresistance is found to increase strongly at low angles. In effect, at the border of this low-angle region rather sharp dips develop, as is marked in Fig. 13 in the 9 T sweep by arrows. A clear Q2D-type of the AMRO is now only observed at higher angles,  $\theta \gtrsim 70^\circ$ , while in the mid-angular range the modulation of the magnetoresistance appears to be more complex. On increasing the field further, 15 T and 20 T, the low-angle hump gradually fades and the curves again become Q2D like.

We start with the pronounced hump in the low-angular range. Such a behavior is definitely not expected for the NM state but is fully in line with our proposal that here the CDW is established due to the orbital effect. This means that the strong magnetoresistance at low tilt angles as well as the dips, marked by the arrows in Fig. 13, originate from the Q1D-type AMRO. The change to the Q2D-type AMRO above  $70^\circ$  we interpret by the reduction of the orbital effect, since the latter only depends on the perpendicular field component. On tilting

the field the CDW energy gap becomes smaller, and with it the magnetic breakdown gap. Therefore, the Q2D-type AMRO must become dominant.

At higher fields, 15 T and 20 T, strong magnetic breakdown sets in, so that even at low angles the AMRO again becomes dominated by the Q2D Fermi surface. This is directly reflected in the quite strong SdH oscillations which are superposed on these curves. Such a behavior is already well known from ambient pressure measurements, where a clear crossover from the Q1D AMRO regime to the Q2D AMRO regime occurs with field due to the magnetic breakdown<sup>47</sup>.

Altogether, the measured AMROs are thus consistent with the results discussed above. Since the hysteretic first order transitions were found to appear already at higher temperatures at the CS field orientations one could also expect some additional features to emerge at these angles. As we have seen in Fig. 9 the first CS angle must be around  $57.7^\circ$ . Although there seem to be some anomalous features in between  $40^\circ - 60^\circ$  in the plots shown in Fig. 13, there is obviously no direct sign of this CS angle. This, however, is not too surprising, since the temperature here is rather high, so that an effect of the CS angle already smears out.

#### IV. CONCLUSION

The presented results provide an evidence that at pressures  $P \gtrsim 2.5$  kbar the CDW in  $\alpha$ -(BEDT-TTF)<sub>2</sub>KHg(SCN)<sub>4</sub> only exists under magnetic field due to the orbital effect. Within this re-entrant CDW state a slow oscillation in the magnetoresistance background of very low frequency is observed. We show that this oscillation displays the new phenomenon of FICDW transitions. Direct evidence for this is given by a clear hysteretic structure observed in the magnetoresistance at perpendicular field direction at  $P = 3$  kbar and  $T = 100$  mK. Moreover, the superposition of the orbital quantization and the Pauli effect for different spin subbands is shown to cause a modulation of the density-wave stability on tilting the magnetic field orientation towards the conducting plane. This is experimentally seen in a sign reversal of the slow oscillation amplitude and, in particular, clear hysteretic structures at elevated temperatures in the vicinity of the CS angle, where the quantized values of the nesting vector for different spin subbands superpose on each other. These observations

demonstrate the existence of FICDW transitions at  $P > P_0$  in this organic conductor.

- 
- <sup>1</sup> T. Ishiguro, K. Yamaji, and G.Saito, *Organic Superconductors, 2<sup>nd</sup> edition* (Springer-Verlag Berlin Heidelberg, 1998).
  - <sup>2</sup> G. M. Danner, P. M. Chaikin, and S. T. Hannahs, *Phys. Rev. B* **53**, 2727 (1996).
  - <sup>3</sup> S. Uji, H. Shinagawa, T. Terashima, T. Yakabe, Y. Terai, M. Tokumoto, A. Kobayashi, H. Tanaka, and H. Kobayashi, *Nature* **410**, 908 (2001).
  - <sup>4</sup> S. Uji, T. Terashima, C. Terakura, T. Yakabe, Y. Terai, S. Yasuzuka, Y. Ymanaka, M. Tokumoto, A. Kobayashi, F. Sakai, et al., *J. Phys. Soc. Jpn.* **72**, 369 (2003).
  - <sup>5</sup> P. M. Chaikin, *J. Phys. I France* **6**, 1875 (1996).
  - <sup>6</sup> N. Biskup, J. A. A. J. Perenboom, J. S. Qualls, and J. S. Brooks, *Solid State Commun.* **107**, 503 (1998).
  - <sup>7</sup> P. Christ, W. Biberacher, M. V. Kartsovnik, E. Steep, E. Balthes, H. Weiss, and H. Müller, *JETP Lett.* **71**, 303 (2000).
  - <sup>8</sup> R. H. McKenzie, cond-mat/9706235, unpublished (1997).
  - <sup>9</sup> P. Foury-Leylekian, S. Ravy, J. P. Pouget, and Müller, *Synth. Met.* **137**, 1271 (2003).
  - <sup>10</sup> D. Andres, M. V. Kartsovnik, W. Biberacher, H. Weiss, E. Balthes, H. Müller, and N. Kushch, *Phys. Rev. B* **64**, 161104(R) (2001).
  - <sup>11</sup> D. Andres, M. Kartsovnik, W. Biberacher, K. Neumaier, E. Schuberth, and H. Müller, *Phys. Rev. B* **72**, 174513 (2005).
  - <sup>12</sup> D. Andres, M. Kartsovnik, P. D. Grigoriev, W. Biberacher, and H. Müller, *Phys. Rev. B* **68**, 201101(R) (2003).
  - <sup>13</sup> N. Harrison, J. Singleton, A. Bangura, A. Ardavan, P. A. Goddard, R. D. MacDonald, and L. K. Montgomery, *Phys. Rev. B* **69**, 165103 (2004).
  - <sup>14</sup> D. Zanchi, A. Bjelis, and G. Montambaux, *Phys. Rev. B* **53**, 1240 (1996).
  - <sup>15</sup> A. G. Lebed, *Pis'ma Zh. Eksp. Teor. Fiz.* **78**, 170 (2003).
  - <sup>16</sup> L. P. Gor'kov and A. G. Lebed, *J. Phys. (Paris) Lett.* **45**, L433 (1984).
  - <sup>17</sup> G. Montambaux, *Phys. Rev. B* **38**, 4788 (1988).
  - <sup>18</sup> J. F. Kwak, J. E. Schirber, P. M. Chaikin, J. M. Williams, H.-H. Wang, and L. Y. Chiang, *Phys. Rev. Lett.* **56**, 972 (1986).

- <sup>19</sup> K. Yamaji, J. Phys. Soc. Jpn. **53**, 2189 (1984).
- <sup>20</sup> G. Montambaux, M. Heritier, and P. Lederer, Phys. Rev. Lett. **55**, 2078 (1985).
- <sup>21</sup> K. Yamaji, J. Phys. Soc. Jpn. **56**, 1841 (1987).
- <sup>22</sup> D. Andres, M. V. Kartsovnik, W. Biberacher, T. Togonidze, H. Weiss, E. Balthes, and N. Kushch, Synth. Met. **120**, 841 (2001).
- <sup>23</sup> M. V. Kartsovnik, D. Andres, W. Biberacher, P. D. Grigoriev, E. A. Schuberth, and H. Müller, J. Phys. IV France **114**, 191 (2004).
- <sup>24</sup> M. V. Kartsovnik, D. Andres, P. D. Grigoriev, W. Biberacher, and H. Müller, Physica B: Condensed Matter **346-347**, 368 (2004).
- <sup>25</sup> M. V. Kartsovnik, A. E. Kovalev, and N. D. Kushch, J. Phys. I France **3**, 1187 (1993).
- <sup>26</sup> R. H. McKenzie, G. J. Athas, J. S. Brooks, R. G. Clark, A. S. Dzurak, R. Newbury, R. P. Starrett, A. Skougarevsky, M. Tokumoto, N. Kinoshita, et al., Phys. Rev. B **54**, 8289(R) (1996).
- <sup>27</sup> A. House, C. J. Haworth, J. M. Caulfield, S. Blundell, M. M. Honold, J. Singleton, W. Hayes, S. M. Hayden, P. Meeson, M. Springford, et al., J. Phys. Cond. Mat. **8**, 10361 (1996).
- <sup>28</sup> N. Harrison, E. Rzepniewski, J. Singleton, P. J. Gee, M. M. Honold, P. Day, and M. Kurmoo, J. Phys.: Condens. Matter **11**, 7227 (1999).
- <sup>29</sup> N. Harrison, N. Biskup, J. S. Brooks, L. Balicas, and M. Tokumoto, Phys. Rev. B **63**, 195102 (2001).
- <sup>30</sup> T. Sasaki and N. Toyota, Solid. State. Commun. **82**, 447 (1993).
- <sup>31</sup> M. V. Kartsovnik, W. Biberacher, E. Steep, P. Christ, K. Andres, A. G. M. Jansen, and H. Müller, Synth. Metals **86**, 1933 (1997).
- <sup>32</sup> M. Honold, N. Harrison, J. Singleton, M.-S. Nam, S. J. Blundell, C. H. Mielke, M. Kartsovnik, and N. Kushch, Phys. Rev. B **59**, 10417(R) (1999).
- <sup>33</sup> N. Harrison, L. Balicas, J. S. Brooks, and M. Tokumoto, Phys. Rev. B **62**, 14212 (2000).
- <sup>34</sup> K. Kajimura, H. Tokumoto, M. Tokumoto, K. Murata, T. Ukachi, H. Anzai, T. Ishiguro, and G. Saito, J. Phys. France **44**, 1059 (1983).
- <sup>35</sup> A. V. Kornilov, V. M. Pudalov, Y. Kitaoka, K. Ishida, T. Mito, J. S. Brooks, J. S. Qualls, J. A. A. J. Perenboom, N. Tateiwa, and T. C. Kobayashi, Phys. Rev. B **65**, 060404(R) (2002).
- <sup>36</sup> W. Kang, S. T. Hannahs, and P. M. Chaikin, Phys. Rev. Lett. **70**, 3091 (1993).
- <sup>37</sup> J. Sólyom, Adv. Phys. **28**, 201 (1979).
- <sup>38</sup> G. Grüner, *Density Waves in Solids* (Addison Wesley, 1994).

- <sup>39</sup> P. Fulde and R. A. Ferrell, Phys. Rev. **135**, A550 (1964).
- <sup>40</sup> A. I. Buzdin and V. V. Tugushev, JETP **58**, 428 (1983).
- <sup>41</sup> P. D. Grigoriev and D. S. Lyubshin, Phys. Rev. B **72**, 195106 (2005).
- <sup>42</sup> A. Bjelis, D. Zanchi, and G. Montambaux, J. Phys. IV France **9**, PR10 (1999).
- <sup>43</sup> D. Shoenberg, *Magnetic oscillations in metals* (Cambridge University Press, 1984).
- <sup>44</sup> J. Wosnitza, *Fermi Surfaces of Low-Dimensional Organic Metals and Superconductors* (Springer-Verlag Berlin Heidelberg, 1996).
- <sup>45</sup> A. E. Kovalev, S. Hill, and J. S. Qualls, Phys. Rev. B **66**, 134513 (2002).
- <sup>46</sup> M. V. Kartsovnik, Chem. Rev. **104**, 5737 (2004).
- <sup>47</sup> A. House, S. Blundell, M. M. Honold, J. Singleton, J. A. A. J. Perenboom, W. Hayes, M. Kurmoo, and P. Day, J. Phys. Cond. Mat. **8**, 8829 (1996).

Fig. 1. Magnetoresistance at various pressures at 100 mK. Above  $P_0 \approx 2.5$  kbar slow oscillations emerge in the magnetoresistance background. With increasing pressure these oscillations gradually move to higher fields as visualized by dashed lines.

Fig. 2. Expanded low field part of the curves from Fig. 1. Above 2.5 kbar the fast SdH oscillations start to appear already below 2 T.

Fig. 3. Magnetoresistance at  $P = 3$  kbar. The data are recorded at increasing field and different temperatures. The curves are offset from each other. At the lowest temperature the down sweep is additionally shown by the black curve. The dashed line marks a field, at which a maximum of the fast SdH oscillations turns at to a minimum on lowering the temperature, that visualizes the phase inversion.

Fig. 4. Magnetoresistance recorded at two different temperatures and  $P = 3.5$  kbar. Note the temperature independent resistance at low fields, suggesting the NM state to be present. As in Fig. 3, the dashed line at higher fields illustrates the phase inversion.

Fig. 5. FFT spectrum of the magnetoresistance at  $T = 100$  mK and  $P = 3.5$  kbar in the field interval 10-15 T. The additional frequencies  $\lambda$  and  $\nu$  within the re-entrant CDW state are clearly resolved.

Fig. 6. FFT spectrum of the whole measured field range; 2-15 T. The slow oscillations are reflected by an additional peak at  $\approx 20$  T

Fig. 7. Up and down field sweeps of the magnetoresistance at  $P = 3$  kbar and  $T = 100$  mK. The hysteresis, determined by subtracting one curve from the other, is shown below. A clear structure matching the oscillatory features can be seen.

Fig. 8. The FICDW transition points at 100 mK move to higher magnetic fields with increasing pressure.

Fig. 9. Field sweeps at different tilt angles of magnetic field, with the field scaled in  $\cos(\theta)$ , at  $T = 0.4$  K,  $P = 2.8$  kbar. The curves at different angles are offset for clarity. Black curves show up sweeps of the magnetic field, grey curves down sweeps. The dashed line marks the position of the FICDW transition for which the observed hysteresis has a maximum.

Fig. 10. Hysteresis obtained from a subtraction of the up from the down sweeps of Fig. 9 at different field directions. The arrow points to the maximum in the hysteresis at the FICDW transition that is marked in Fig. 9 by the dashed line.

Fig. 11. Field sweeps at  $T = 0.4$  K, as in Fig. 9, in a bigger angular range. To illustrate the presence of "spin zeros", dashed lines are approximately placed at the extrema of the slow oscillations. On increasing the angle the oscillations show several times a change of the amplitude sign.

Fig. 12. Observed angular ranges of the spin zeros scaled according to Eq. (2). The expected linear behaviour of the half odd integer quantum number in  $1/\cos$  allows an evaluation of the CS field directions at integer quantum numbers, Eq. (3).

Fig. 13. Angle-dependent magnetoresistance oscillations for several different fields at 0.7 K and 2.8 kbar. The curves are offset from each other. At 1 T the resistance has been multiplied by 20. The arrows point to the sharp dips, typical of the CDW state, in the curve at 9 T.

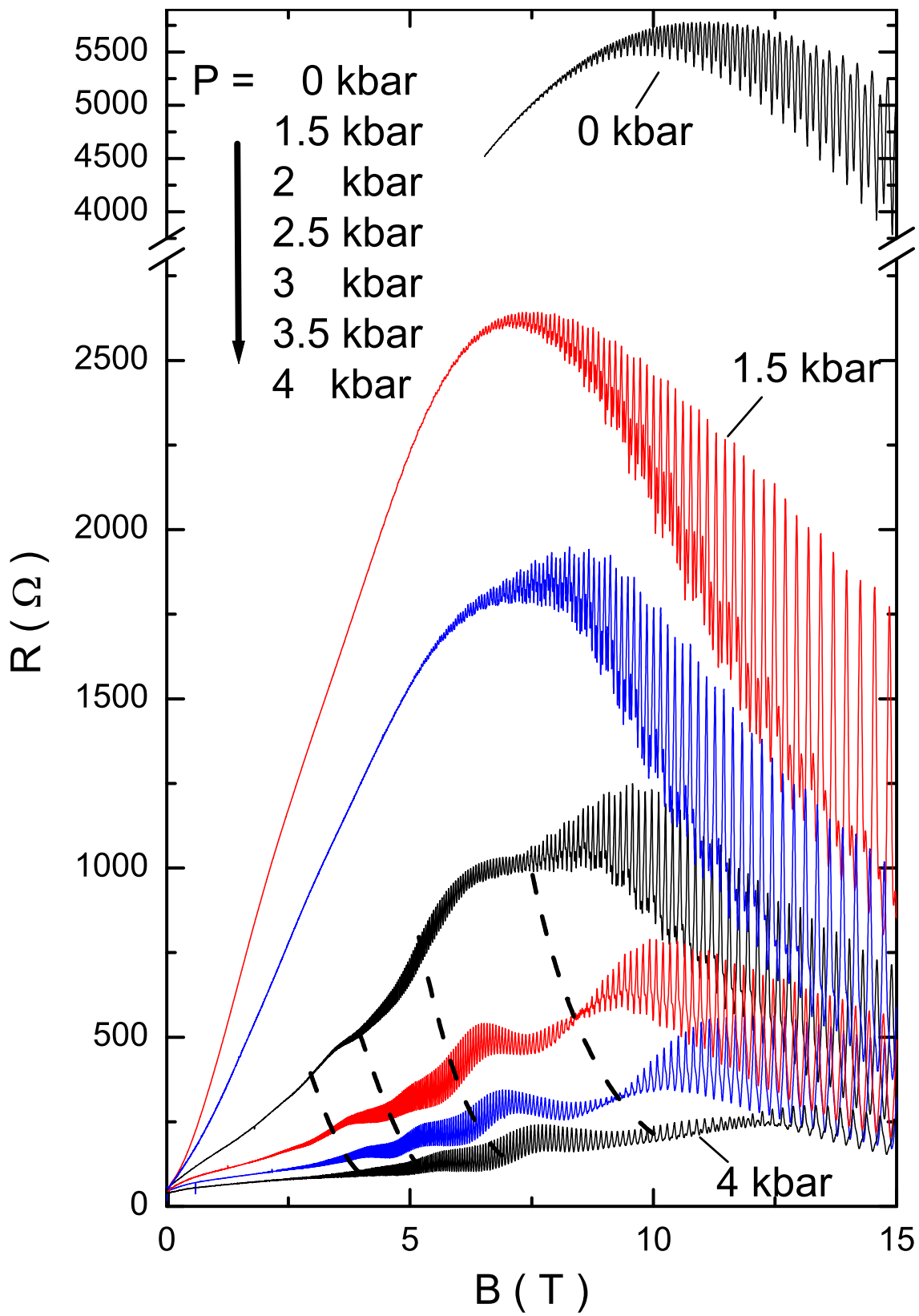


Fig.1 of Andres et al.

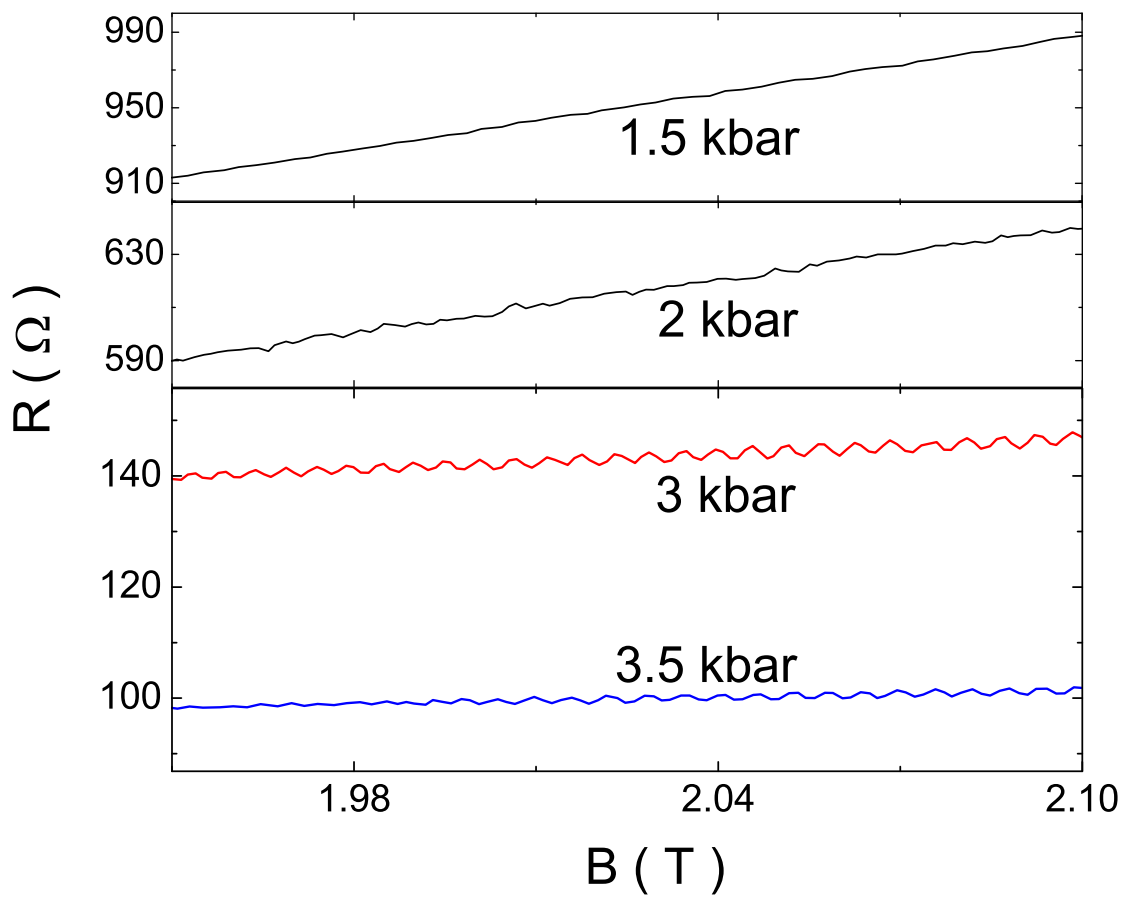


Fig. 2 of Andres et al.

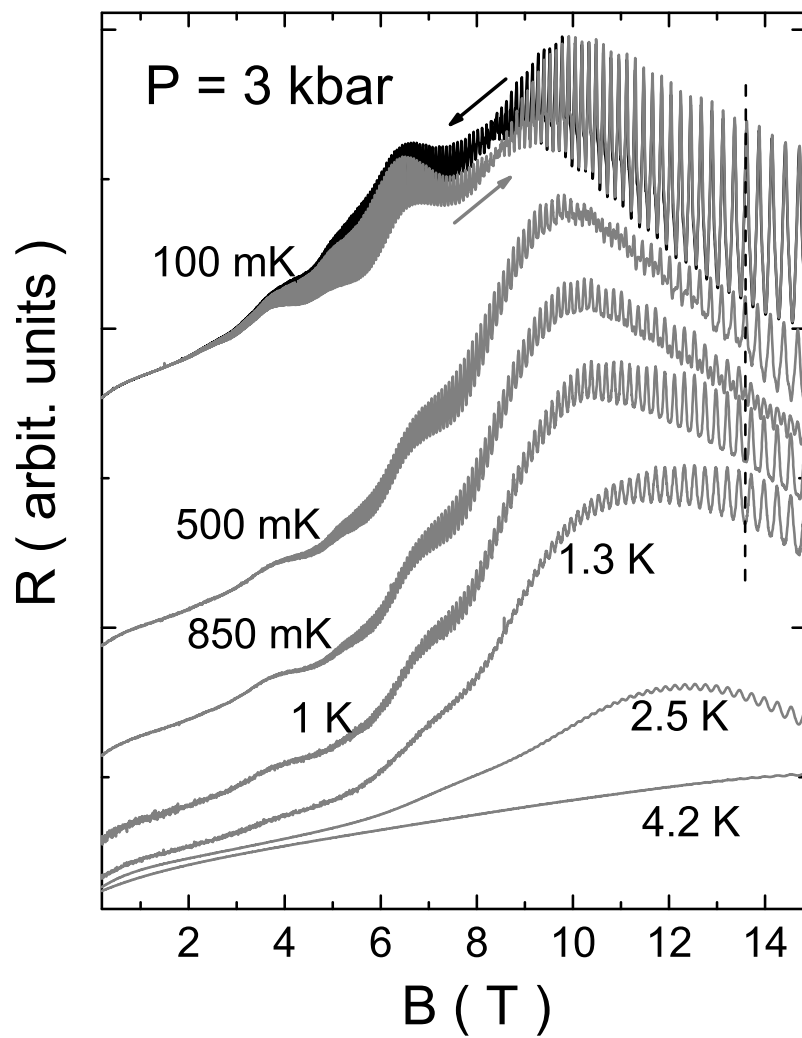


Fig. 3 of Andres et al.

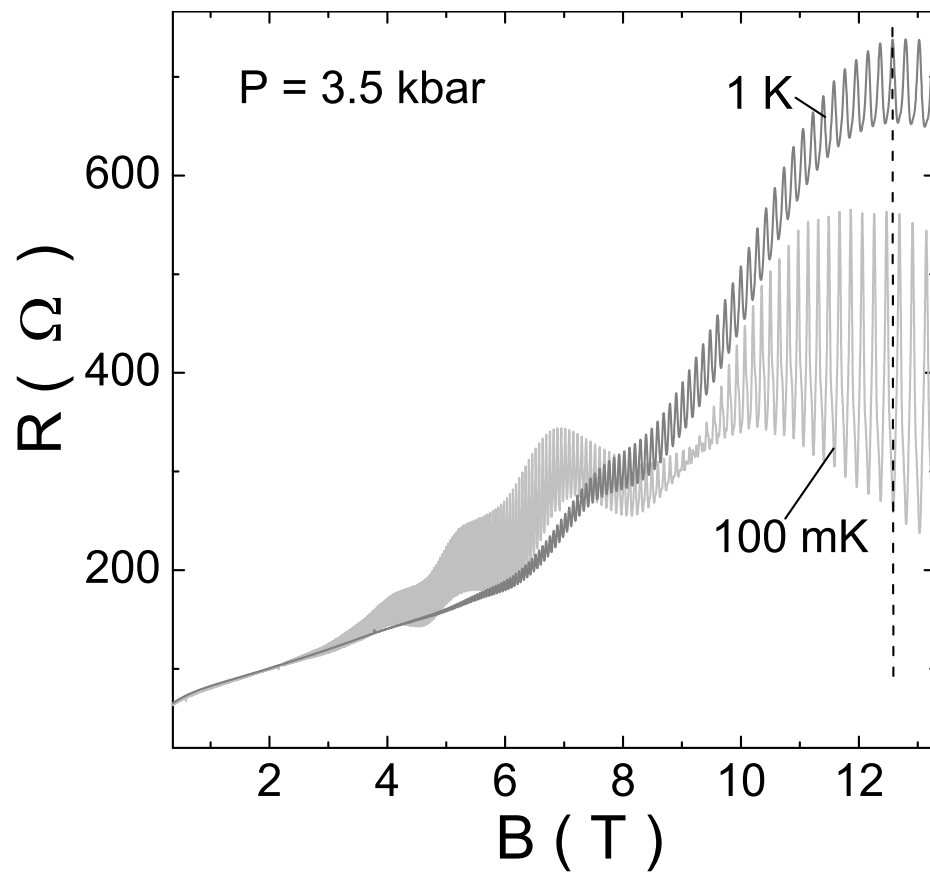


Fig. 4 of Andres et al.

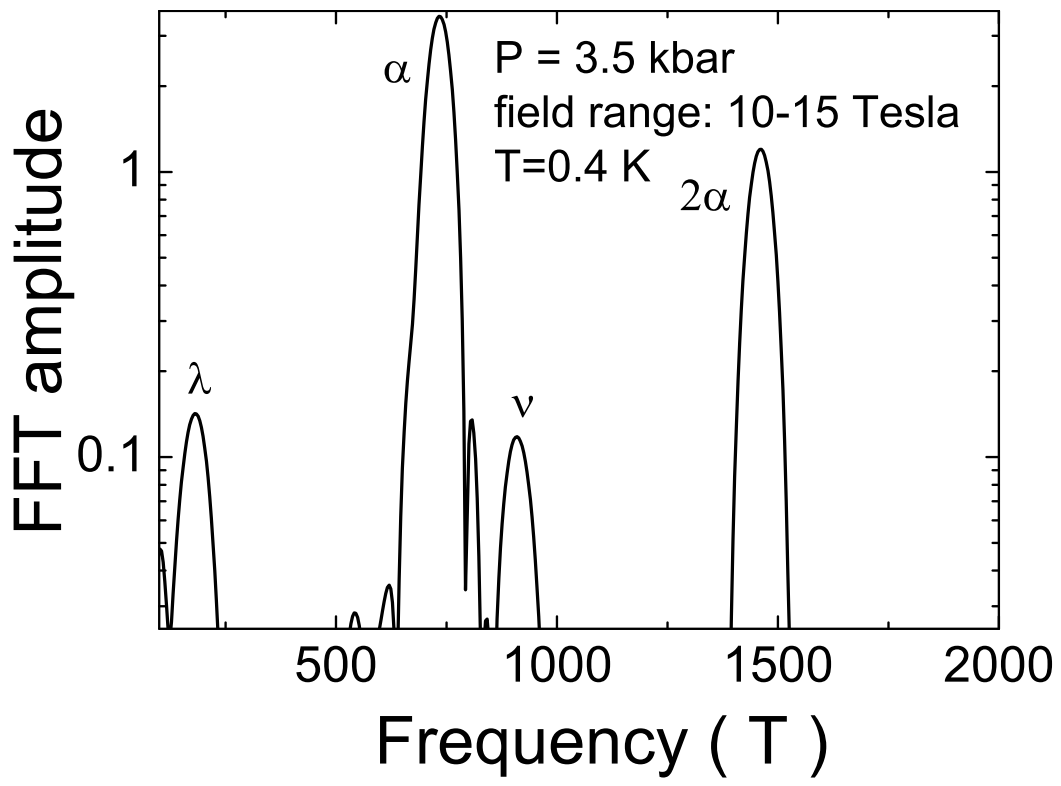


Fig. 5 of Andres et al.

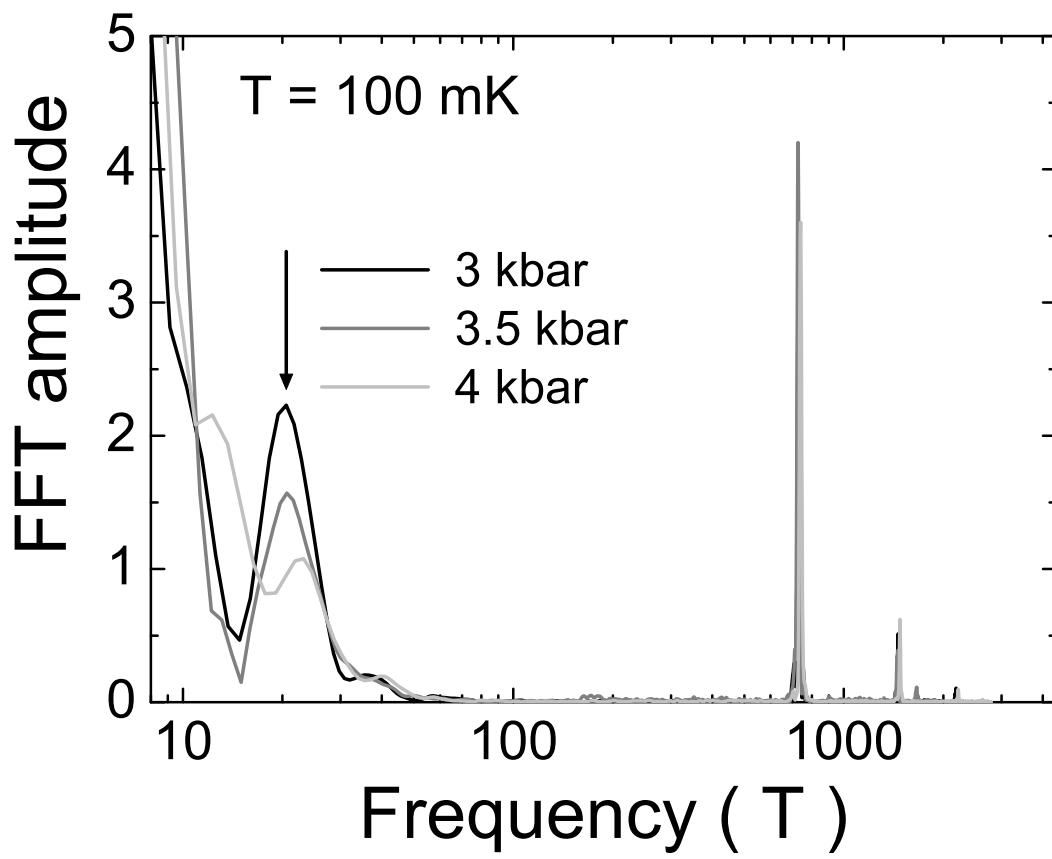


Fig. 6 of Andres et al.

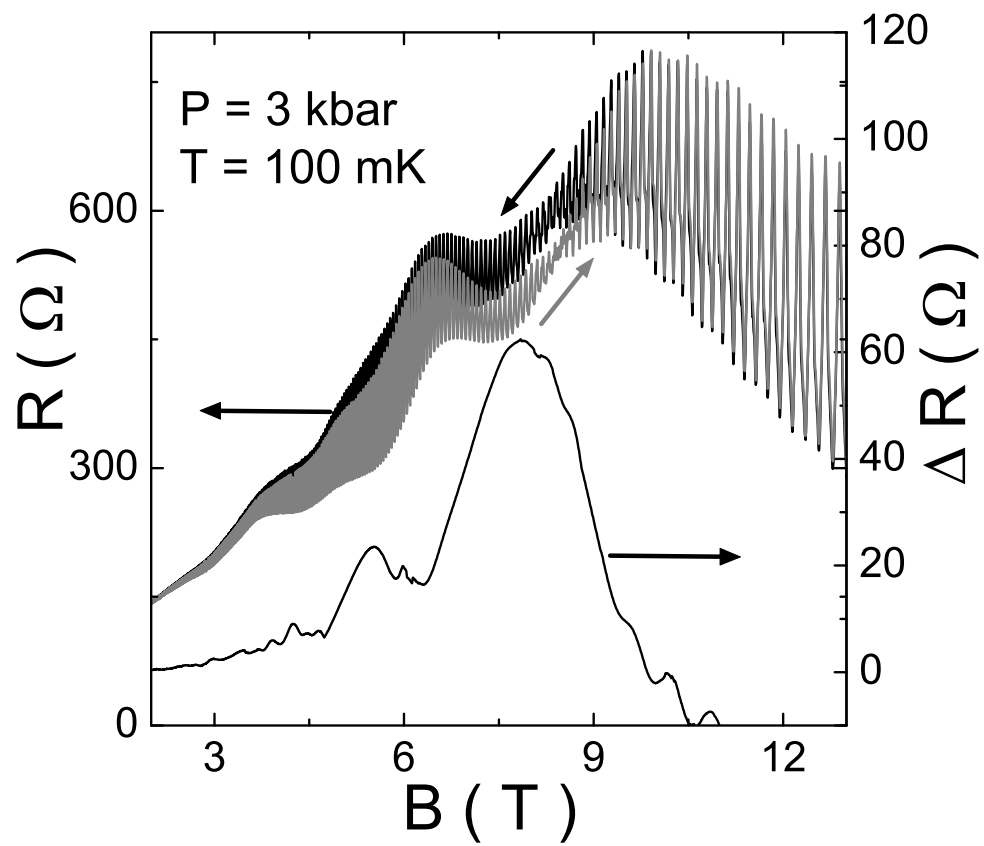


Fig. 7 of Andres et al.

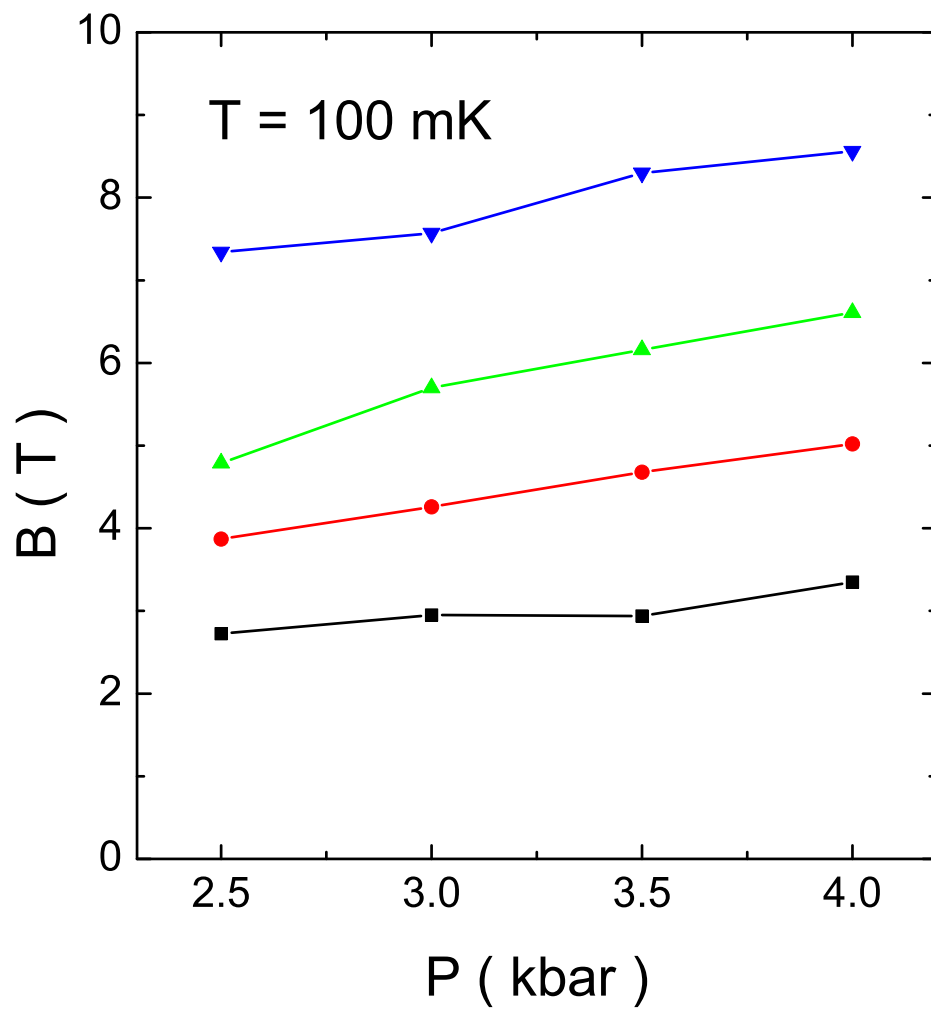


Fig. 8 of Andres et al.

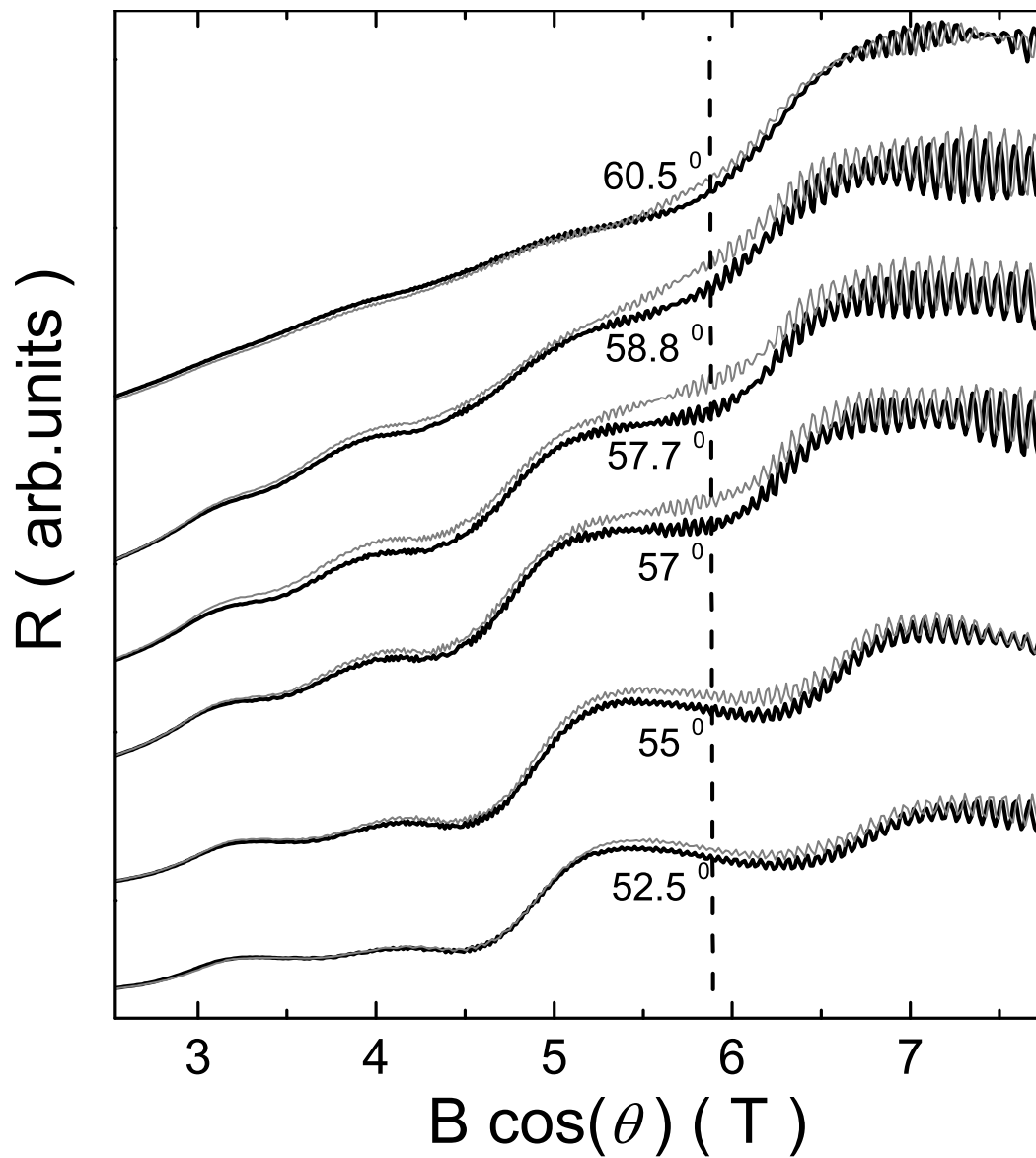


Fig. 9 of Andres et al.

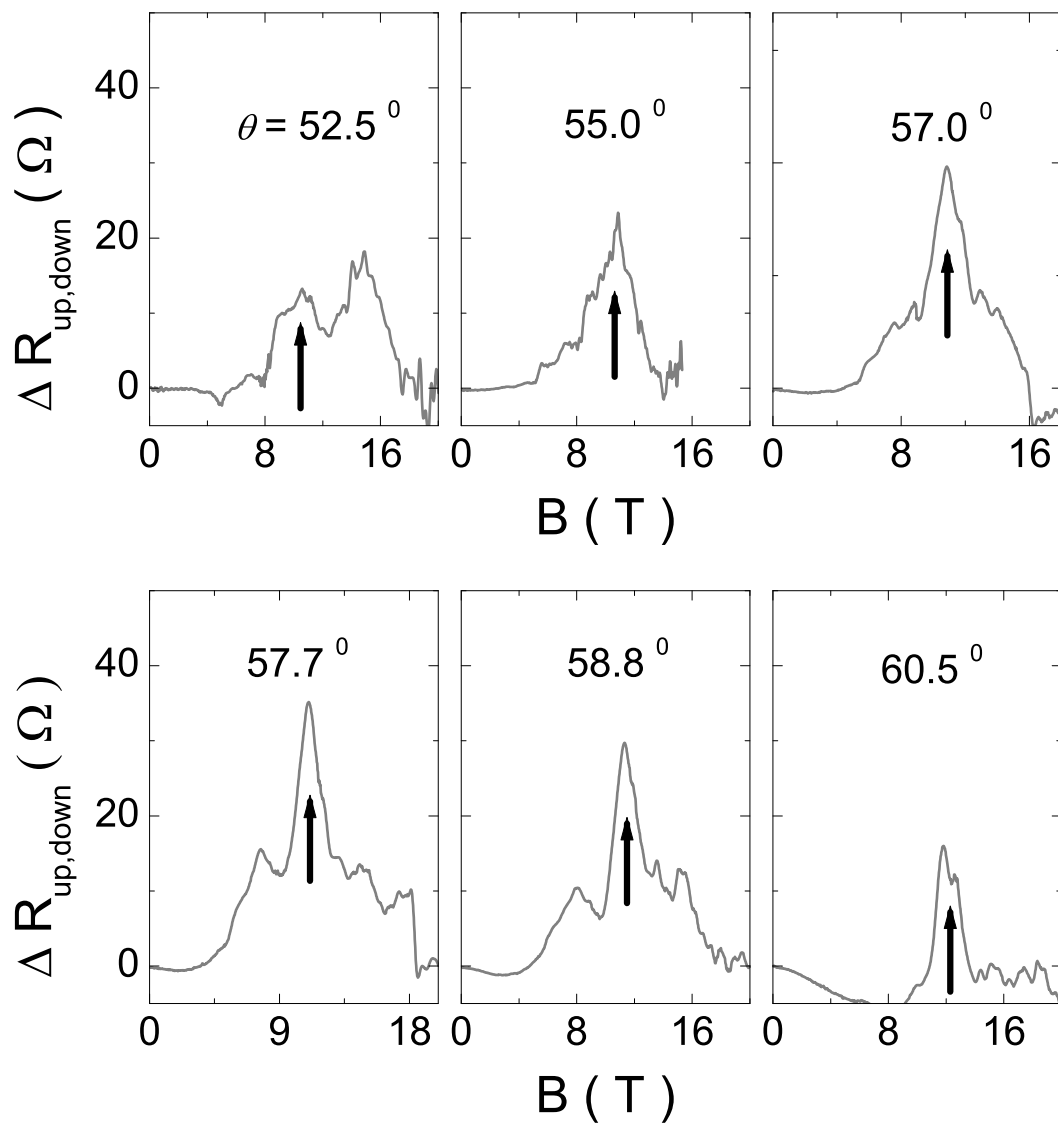


Fig. 10 of Andres et al.

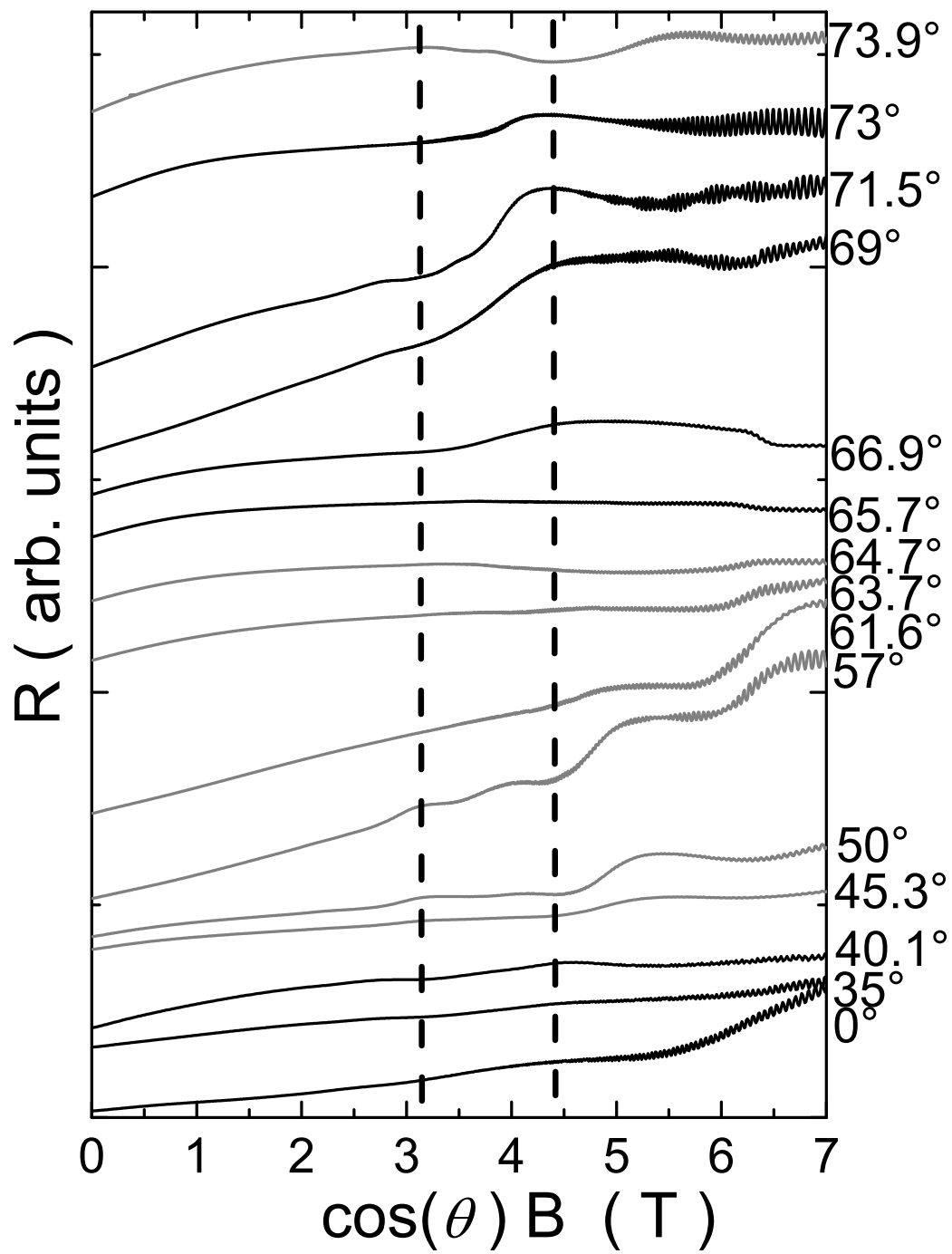


Fig. 11 of Andres et al.

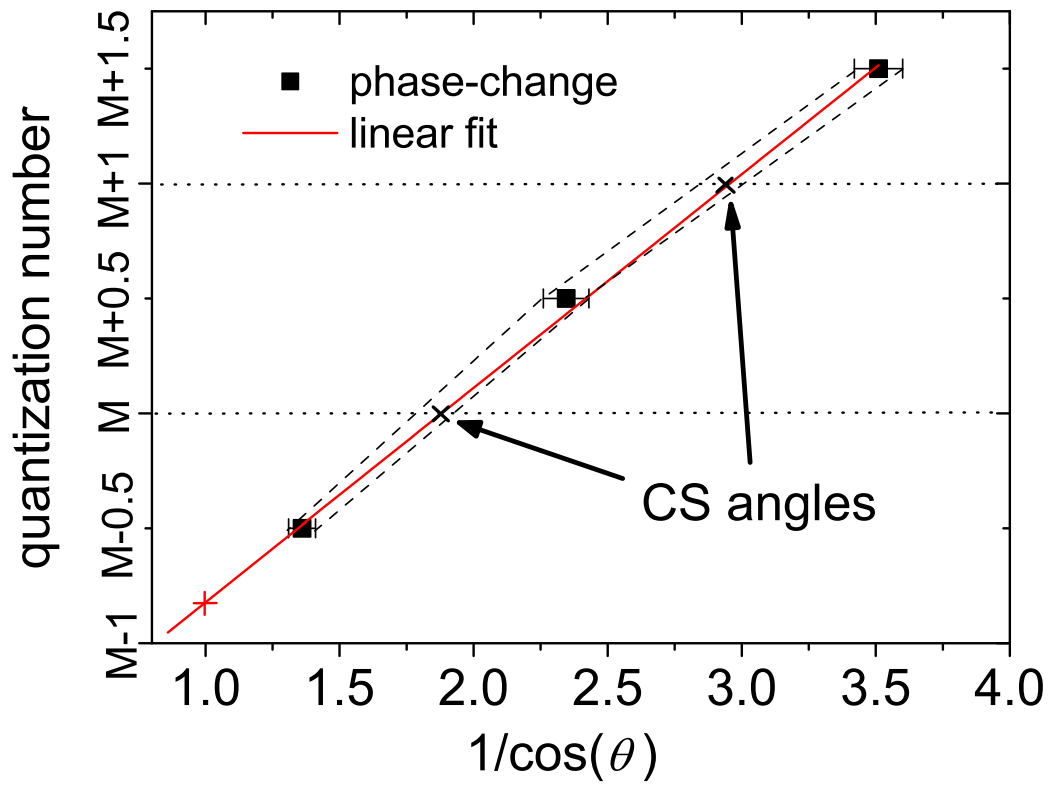


Fig. 12 of Andres et al.

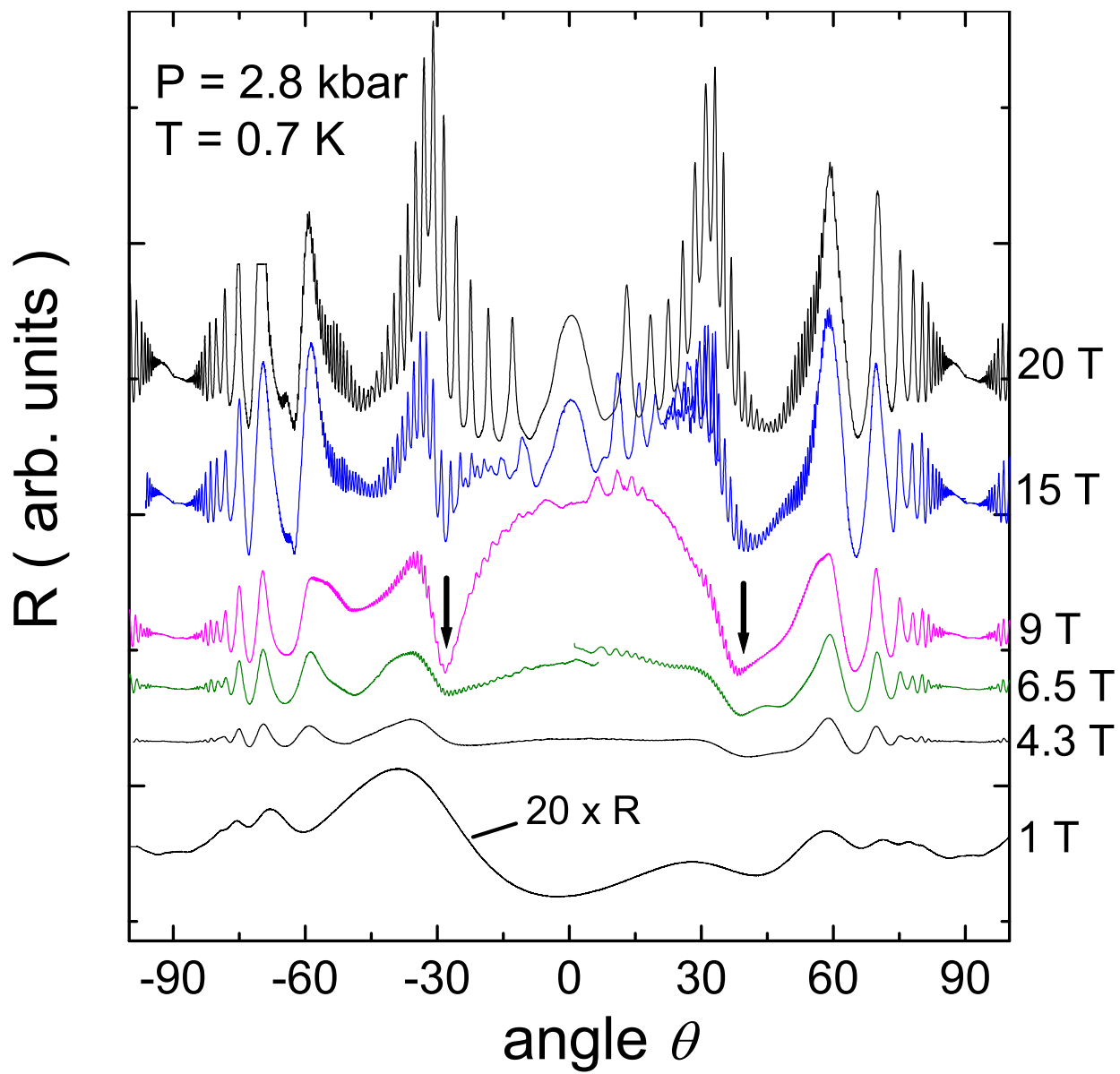


Fig. 13 of Andres et al.